University Library

A gateway to Melbourne's research publications

Minerva Access is the Institutional Repository of The University of Melbourne

Author/s:
Shen, H;Chen, Y;Hu, Y;Ran, L;Lam, SK;Pavur, GK;Zhou, F;Pleim, JE;Russell, AG

Title:
Intense Warming Will Significantly Increase Cropland Ammonia Volatilization Threatening Food Security and Ecosystem Health

Date:
2020-07-24

Citation:
Shen, H., Chen, Y., Hu, Y., Ran, L., Lam, S. K., Pavur, G. K., Zhou, F., Pleim, J. E. & Russell, A. G. (2020). Intense Warming Will Significantly Increase Cropland Ammonia Volatilization Threatening Food Security and Ecosystem Health. One Earth, 3 (1), pp.126-134. https://doi.org/10.1016/j.oneear.2020.06.015.

Persistent Link:
https://hdl.handle.net/11343/252495

License:
cc-by

One Earth

Article

Intense Warming Will Significantly Increase Cropland Ammonia Volatilization Threatening Food Security and Ecosystem Health

Graphical Abstract

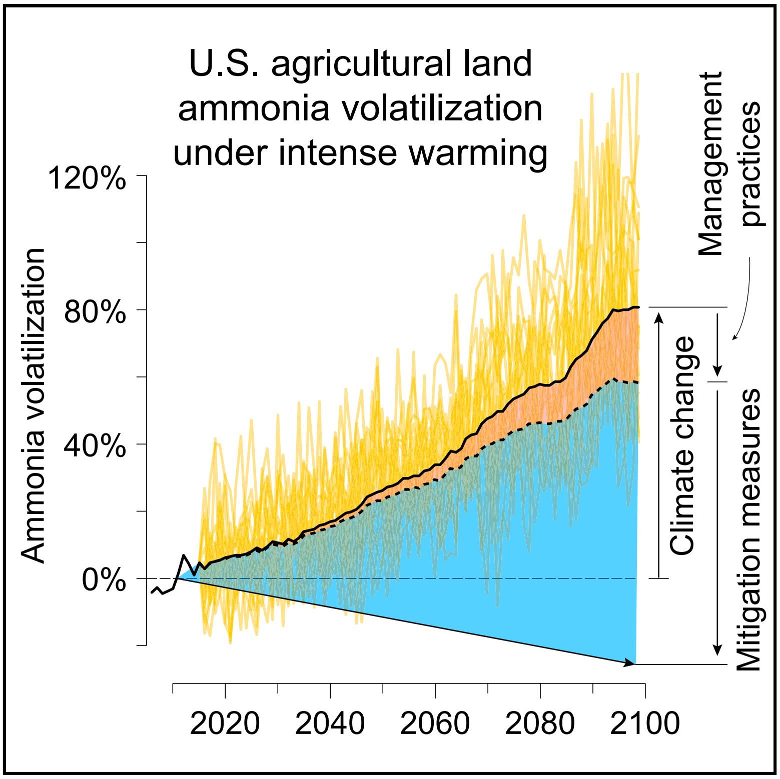

Highlights

- By 2100 warming will increase US agricultural land ammonia emissions by up to 81%
- This increasing trend will be associated with significant reduction in crop yields
- It will increase ammonia concentrations in the air and subsequent deposition
- Feasible control strategies can completely offset this trend under global warming

Authors

Huizhong Shen, Yilin Chen, Yongtao Hu, ..., Feng Zhou, Jonathan E. Pleim, Armistead G. Russell

Correspondence

hshen73@gatech.edu

In Brief

Humans, through agricultural fertilizer application, inject more reactive nitrogen (N_r) to terrestrial ecosystems than do natural sources. Ammonia volatilization is a major pathway of agricultural N_r loss. Using a process-based dynamic model, Shen et al. show that ammonia volatilization from agricultural land in the US will increase by up to 81% by the end of this century due to climate change alone, posing threats to food security, air quality, and ecosystem health, but mitigation strategies are available.

Shen et al., 2020, One Earth *3*, 126–134
July 24, 2020 © 2020 The Author(s). Published by Elsevier Inc.
https://doi.org/10.1016/j.oneear.2020.06.015

CellPress

CellPress OPEN ACCESS

Gold Standard for the Global Goals
3 tons of CO_2 offset

One Earth

Article

Intense Warming Will Significantly Increase Cropland Ammonia Volatilization Threatening Food Security and Ecosystem Health

Huizhong Shen,[1,6,*] Yilin Chen,[1] Yongtao Hu,[1] Limei Ran,[2,5] Shu Kee Lam,[3] Gertrude K. Pavur,[1] Feng Zhou,[4] Jonathan E. Pleim,[2] and Armistead G. Russell[1]

[1]School of Civil & Environmental Engineering, Georgia Institute of Technology, Atlanta, GA 30332, USA
[2]National Exposure Research Laboratory, United States Environmental Protection Agency, Research Triangle Park, NC 27711, USA
[3]School of Agriculture and Food, Faculty of Veterinary and Agricultural Sciences, the University of Melbourne, Melbourne, VIC 3010, Australia
[4]Sino-French Institute for Earth System Science, Laboratory for Earth Surface Processes, College of Urban and Environmental Sciences, Peking University, Beijing 100871, China
[5]Present address: Natural Resources Conservation Service, United States Department of Agriculture, Greensboro, NC 27401, USA
[6]Lead Contact
*Correspondence: hshen73@gatech.edu
https://doi.org/10.1016/j.oneear.2020.06.015

SCIENCE FOR SOCIETY Ammonia (NH_3) loss from fertilized agricultural land has significant environmental and economic consequences. Using an integrated model, we showed that, under an intensely warming climate scenario, agricultural land NH_3 emissions will increase by about 80% in the US by the end of this century because of climate change alone, posing a serious threat to crop production, air quality, and ecosystem health. We found that a combination of climate-adaptive agricultural management practices with attainable mitigation measures can completely offset the warming-induced increment in NH_3 emissions and improve crop production, air quality, and ecosystem health.

SUMMARY

Cropland ammonia volatilization ($V_{NH3,AG}$) is a major pathway of agricultural nitrogen loss. It remains unclear, however, how climate warming and human intervention (e.g., agricultural management) will affect $V_{NH3,AG}$. Here, we use a fully coupled agroecosystem/chemical transport model and multiple climate projections to quantify the changes in climate-induced $V_{NH3,AG}$ over the US. We show that climate change under an intensely warming scenario will increase $V_{NH3,AG}$ by 81% (95% confidence interval, 69%–92%) from 2010 to 2100. The increase in $V_{NH3,AG}$ will cause a 10% loss of nitrogen applied, decrease crop yields by 540 Gg-N year^{-1}, increase atmospheric burden of ammonia/ammonium by 18%, and increase ammonia/ammonium deposition to sensitive ecosystems by 14%. We have found that combining climate-adaptive agricultural practices with feasible mitigation measures can fully offset the warming-induced increase in $V_{NH3,AG}$, saving 13% of applied nitrogen, increasing yields by 735 Gg-N year^{-1}, and providing net benefits for air quality and ecosystem health.

INTRODUCTION

Ammonia (NH_3) in the air is the key constituent controlling and stabilizing aerosol acidity[1–3] and is a major contributor to secondary aerosol that has adverse impacts on human health and climate.[3–6] Excessive NH_3 deposition is harmful to sensitive ecosystems as it causes soil acidification, eutrophication, and biodiversity loss.[7–11] Globally, approximately 43% of the atmospheric NH_3 emission is attributed to volatilization from soils and plants over fertilized agricultural land ($V_{NH3,AG}$)[12] due to the application of synthetic fertilizer and manure (agricultural land here refers to the cultivated land used for growing crops, hay, and pasture; $V_{NH3,AG}$ in this study denotes the NH_3 volatilization from application of fertilizer and manure; $V_{NH3,AG}$ does not includes other livestock management processes except land application of manure). Currently, 10%–20% of the agricultural nitrogen (N) applied worldwide is lost via $V_{NH3,AG}$ with important consequences for the global N cycle.[13–15]

$V_{NH3,AG}$ may increase as climate warms[12,16–19] because warmer conditions are thermodynamically favorable for increased NH_3 release from multiple surface layers (e.g., soil and stomatal and moisture layers on the leaf cuticle) regulated

 © 2020 The Author(s). Published by Elsevier Inc.
This is an open access article under the CC BY license (http://creativecommons.org/licenses/by/4.0/).

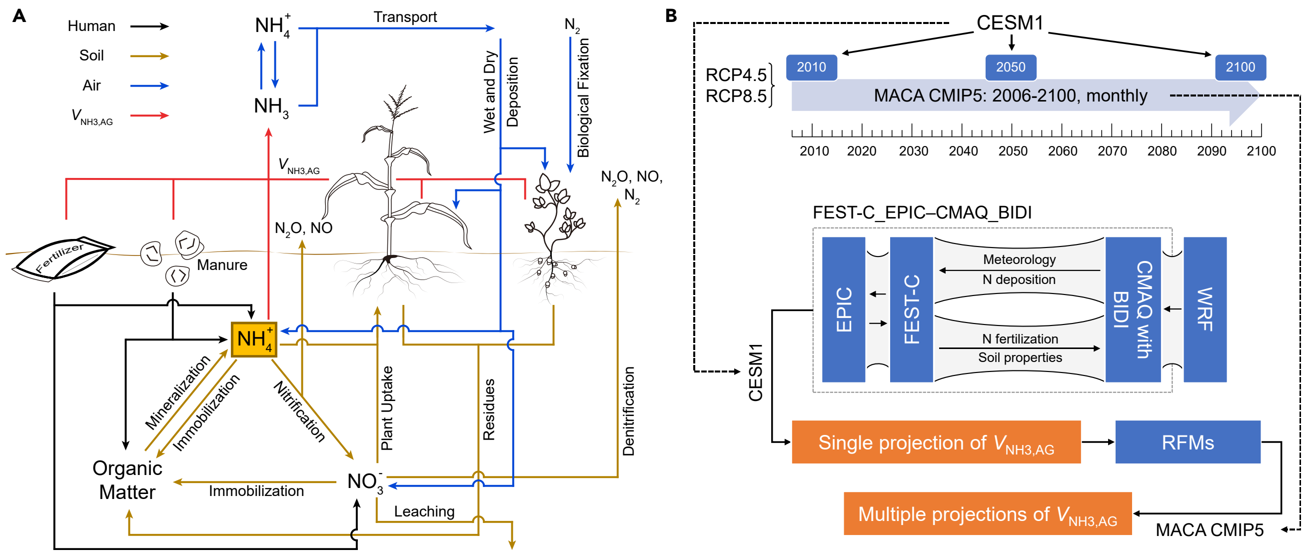

Figure 1. Study Design

(A) Schematic of the key processes associated with estimating $V_{NH3,AG}$ and the downstream impacts. N flows stemming from different media (e.g., soils, atmosphere, and human activities) are marked in different colors with $V_{NH3,AG}$ marked in red.

(B) Flow chart of the integrated modeling framework (Experimental Procedures). FEST-C_EPIC–CMAQ_BIDI, the fully coupled agroecosystem/chemical transport model; WRF, the Weather Research and Forecasting model; CMIP5, Phase 5 of the Coupled Model Intercomparison Experiment; CESM1, the global bias-corrected CMIP5 output data from the National Center for Atmospheric Research's Community Earth System Model version 1; MACA CMIP5, Multivariate Adaptive Constructed Analogs CMIP5 statistically downscaled data containing 18 climate model projections; RFMs, reduced-form models developed based on the FEST-C_EPIC–CMAQ_BIDI output) see the main text for EPIC, FEST-C, CMAQ, BIDI, RCP4.5, and RCP8.5.

by the Henry's Law equilibrium and the NH_3/ammonium (NH_4^+) dissociation equilibrium.[20–22] As a major pathway of agricultural N loss, increased $V_{NH3,AG}$ will likely undermine global efforts to improve agricultural nitrogen use efficiency. However, how regional-to-global $V_{NH3,AG}$ responds to climate change remains a challenging question[12] because changing climate alters not only the physical, chemical, and biochemical processes of NH_3 air-surface bidirectional exchange, but also the soil and atmospheric properties, plant biology, and agricultural management practices. Increased soil temperature (1) increases the solubility of urea,[23] (2) can increase the rates of nitrification and denitrification, which consumes NH_4^+ and nitrate, respectively, leading to the loss of soil reactive N (N_r, which includes both oxidized and reduced N species, such as nitrate and NH_4^+),[24,25] and (3) alters soil pH,[26] which affects the NH_3/NH_4^+ equilibrium.[20] Ambient NH_3 concentrations and deposition responding to $V_{NH3,AG}$ changes reveal negative and positive feedback, respectively. NH_3 deposition (as a soil N source) enhances $V_{NH3,AG}$, and ambient NH_3 concentrations suppress $V_{NH3,AG}$ by increasing cuticular resistances.[27] Management practices, such as the type, amount, timing, and methods of N application will also evolve under climate change, which further complicates the climate dependency of $V_{NH3,AG}$.[12] A quantitative assessment of $V_{NH3,AG}$'s dependency on future climate change requires integrating the dynamics and interactions of plants, soils, atmosphere, and human activities.[12]

Past studies used empirical relationships between climatic drivers and NH_3 volatilization in natural circumstances (e.g., seabird colonies) to project future changes in $V_{NH3,AG}$ due to climate change.[12] However, $V_{NH3,AG}$ differs from NH_3 volatilization over non-agricultural land that naturally occurs because human intervention plays a critical role in $V_{NH3,AG}$. So far, few studies have used process-based dynamic models to evaluate the changes in $V_{NH3,AG}$ in response to future climate change.[28] Here, we use a process-based fully coupled agroecosystem-air quality model, FEST-C_EPIC–CMAQ_BIDI,[29–32] to elucidate the climate change impacts on future $V_{NH3,AG}$ in the US, one of the nations with the largest coverage of agricultural land (Figure 1).[33]

Our model, FEST-C_EPIC–CMAQ_BIDI, consists of an agroecosystem model (Environmental Policy Integrated Climate [EPIC] model) and a chemical transport model (Community Multiscale Air Quality model [CMAQ]) using an interface (the Fertilizer Emission Scenario Tool for CMAQ [FEST-C]) and an NH_3 bidirectional exchange module (BIDI) to couple the two models (Experimental Procedures).[32] For $V_{NH3,AG}$, we consider both synthetic fertilizer and manure application, which is estimated to contribute 30% of the total NH_3 emission in the US in 2011 (Table S1). FEST-C_EPIC simulates 42 rain-fed and irrigated crops (e.g., corn grain and soybean) and grasses (e.g., hay and alfalfa) (Table S2) and considers various fertilizer types (see Data and Code Availability) and application methods.[34,35] FEST-C_EPIC–CMAQ_BIDI simultaneously assesses the responses of multi-media environmental processes and agricultural management practices to climate change and is expected to be a suitable tool to investigate the climate dependency of $V_{NH3,AG}$ (Figure 1). We consider two climate scenarios comprised of the Representative Concentration Pathway (RCP) 4.5 (a climate scenario showing a moderate increasing trend in temperature) and RCP8.5 (a climate scenario showing an intensely increasing trend in temperature). Based on the integrated modeling framework, we evaluate the effectiveness of mitigation strategies for reducing $V_{NH3,AG}$. These strategies include adaptation of management practices (i.e., amount and timing of fertilizer application) to climate change and deployment of mitigation measures (comprised of replacement of urea with non-urea fertilizers [RU], urea application with irrigation [UIR], application of urease inhibitor [UIN], and deep placement of fertilizers [DP]).

RESULTS

Observed Climate Dependency of $V_{NH3,AG}$

Satellite retrievals suggest an increasing trend (+40%) in NH_3 concentration across the Midwest agricultural region (35°N–45°N, 87°W–101°W) during the last 13 years (Figure S1).[16] The expansion of agricultural land (+0.5%) and an increasing use of fertilizer (+8%) can partly explain this increase in NH_3 concentration.[16,36] Reductions in NO_X and SO_2 emissions have played a minor role, given that Reductions in NO_X and SO_2 emissions have played a minor role, given that no significant trend in the observed NH_3 levels is found in the eastern US despite large emission reductions in NO_X and SO_2.[1] On the other hand, the interannual NH_3 variation from which the long-term trend is removed by detrending, shows a significantly positive correlation with annual mean 2-m temperature and a negative correlation with total precipitation ($p < 0.05$) (Figure S1), which indicates a potential climate dependency. Satellite retrievals suggest that, in 2012, NH_3 concentrations in the Midwest reached their highest levels, which coincides with the highest temperature on record and dryer-than-normal conditions.[37] Consistent with the space-based observations, ground measurements operated by the Ammonia Monitoring Network peaked in 2012 at eight of the ten sites within this region (Figure S2).[38]

The occurrence of high NH_3 levels in 2012 could be attributed to emissions, gas-particle partitioning, and reduced removal processes that link to the abnormal climate conditions. To determine to what extent emission changes contributed to the NH_3 level raise, we conduct simulations based on FEST-C_EPIC–CMAQ_BIDI. Compared with CMAQ simulations without coupling the agroecosystem feedbacks, simulations of FEST-C_EPIC–CMAQ_BIDI show better agreement with observations—the Normalized Mean Biases of annual mean NH_3 concentrations and NH_4^+ wet and dry deposition reduce from −52% to −30%, −47% to −32%, and −14% to −5%, respectively (Figures S3 and S4; Table S3) (Supplemental Information for more details on model evaluation). By comparing the modeled NH_3 concentrations between 2011 (a year with generally normal temperature and precipitation levels over the Midwest agricultural region) and 2012, we estimate the sensitivities of NH_3 concentration to 2-m temperature ($S_{C,T}$), which average +0.18 ppb K^{-1} in the Midwest and +0.33 ppb K^{-1} at the site locations, in line with the $S_{C,T}$ values derived from space and ground-level observations (+0.15 and +0.34 ppb K^{-1}, respectively). FEST-C_EPIC–CMAQ_BIDI estimates a 20% increase in $V_{NH3,AG}$ (from 400 to 480 Gg-NH_3 year^{-1}) between the two years that is solely caused by changes in meteorology. To isolate the emission-related impact, we turned off the agroecosystem feedbacks and applied the 2011 $V_{NH3,AG}$ to the 2012 simulation. The simulation shows a 40% reduction in $S_{C,T}$, meaning that the $V_{NH3,AG}$ increase is responsible for about 40% of the large-scale increase in NH_3 concentrations (Figure S5). The contribution can be up to 90% in certain areas of the Midwest. This analysis highlights the important role of $V_{NH3,AG}$ leading to the observed NH_3 pulse in 2012 and also supports the suitability of FEST-C_EPIC–CMAQ_BIDI in capturing the NH_3 air-surface dynamics in response to climate change.

Increased $V_{NH3,AG}$ under Future Climate Warming

We use FEST-C_EPIC–CMAQ_BIDI to address the $V_{NH3,AG}$ response under future climate change. The meteorological fields used to drive FEST-C_EPIC–CMAQ_BIDI are generated by downscaling the bias-corrected climate projections generated by the National Center for Atmospheric Research's Community Earth System Model version 1 (CESM1).[39] We conduct FEST-C_EPIC–CMAQ_BIDI simulations under climate conditions of the 2010 (2008–2012), 2050 (2048–2052), and 2100 (2096–2100) periods (Experimental Procedures). To avoid bias caused by climate anomalies, each period is delineated by a 5-year simulation. To isolate the direct impact of climate change, land cover (LC) distributions and CO_2 concentrations for this set of simulations remain unchanged (a brief discussion on the potential impacts of future changes in LC and CO_2 concentration on $V_{NH3,AG}$ can be found in the Supplemental Information). In the RCP4.5 climate scenario, the projected $V_{NH3,AG}$ shows an average increase of 12% and 23% by 2050 and 2100 compared with 2010, respectively, over the CONUS (Table S4). Substantial increases are found in the Northern and Southern Plains (26% and 35% by 2100) and the Corn Belt (23%), while emissions in the eastern and western coastal regions show lower increases (Northeast −1%, Appalachia 7%, Southeast 12%, and Pacific 7%) (see Figure S6 for a map of the 10 farm production regions used in this study). In the RCP8.5 scenario, the projected $V_{NH3,AG}$ shows a striking increase of 59% by 2100, with higher increases occurring in the Southern Plain (82%) and the Corn Belt (79%) and increases of >50% in all other regions except the Pacific (43%) and the Northeast (39%) (Table S4). Mean differences in $V_{NH3,AG}$ between 2010 and 2100 RCP8.5 simulations (+658 Gg-NH_3 year^{-1}) are significantly higher than the standard deviations within each period (90 and 70 Gg-NH_3 year^{-1} for 2010 and 2100 periods, respectively) (Table S4), suggesting a persistent long-term increase despite well-marked interannual variations.

Based on the simulations, we develop three reduced-form models (RFMs) to decompose the spatiotemporal variations in $V_{NH3,AG}$ into various factors, including LC types, climate factors, and agricultural management practices (Experimental Procedures). The first RFM (LC-based RFM) solely uses LC types to determine $V_{NH3,AG}$; the second RFM (RFM_C) builds on the LC-based RFM to include interannual climate variation; the third RFM ($RFM_{C,M}$) further includes agricultural management practices (Experimental Procedures). The performances of these three RFMs are discussed below. The LC-based RFM explains 68% (R^2) of the spatial variation. All types of vegetated land are subject to NH_3 volatilization (V_{NH3} denotes NH_3 volatilization from any type of vegetated land).[40] The regression coefficients (α) representing emission intensities vary by more than two orders of magnitude across different LC types (Figure S7). $V_{NH3,AG}$ generally shows much higher emission intensities than NH_3 volatilization from non-agricultural land. The highest emission

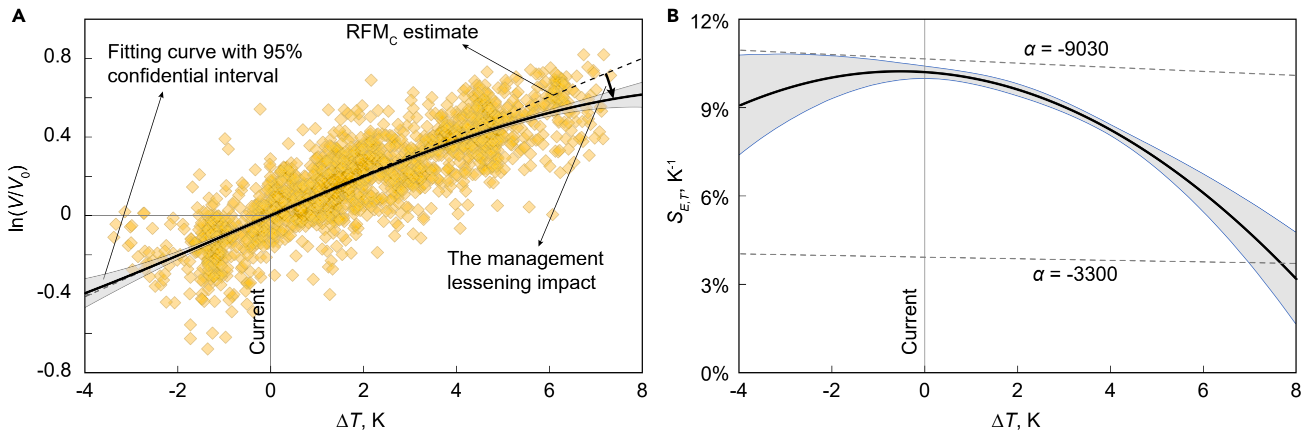

Figure 2. The Increase in $V_{NH3,AG}$ due to Future Warming

(A) The response of $V_{NH3,AG}$ to long-term T change simulated by FEST-C_EPIC–CMAQ_BIDI. Changes in $V_{NH3,AG}$ are expressed as the log-transformed increase rate of $V_{NH3,AG}$, i.e., $\ln(V/V_0)$. Each diamond is associated with a grid cell of which 90% area or more is covered by agricultural land. ΔT represents the long-term T change which is calculated as the difference between future and current annual mean T for each grid cell and period. In addition, we include a specific year in the current period that shows the lowest $V_{NH3,AG}$ levels in order to capture the $V_{NH3,AG}$ trend at negative ΔT levels. The trend is fitted with a cubic polynomial curve. The fitting curve and its 95% confidence interval are illustrated using a solid black line with gray shaded area in the panel. For comparison purposes, the trend estimated by RFM$_C$ is shown as a dashed line. Also see Figure S11, a similar figure for non-agricultural land.

(B) The relation between $S_{E,T}$ and ΔT is marked as a solid black line showing a declining trend of $S_{E,T}$ with T increase over agricultural land. The gray shaded area represents the 95% confidence interval. The lower ($\alpha = -3{,}300$) and higher ($\alpha = -9{,}030$) bounds suggested by Sutton et al.[12] are shown using dashed lines. In 2010, our estimated $S_{V,T}$ for agricultural land (10.2%) is close to the higher bound, suggesting a high sensitivity of $V_{NH3,AG}$ to warming due, in part, to the inclusion of atmospheric feedbacks—with all else equal, an increase in $V_{NH3,AG}$ leads to an increase in ambient NH_3 concentration and thus in NH_3 deposition, which creates a positive feedback for the $V_{NH3,AG}$ increase. In response to the suppression effect of management practices, $S_{V,T}$ gradually decreases to the lower bound as T increases.

intensities are found for rice (18.7 kg-NH_3 ha^{-1} year^{-1}) and cotton fields (12.0 kg-NH_3 ha^{-1} year^{-1}) due to high N fertilizer input for crop growth.[41,42] The lowest is found over forest (0.2 kg-NH_3 ha^{-1} year^{-1}). Overall, $V_{NH3,AG}$ dominates (>80%) the V_{NH3} in the CONUS (Supplemental Information for more details).

We calculate the ratios of the FEST-C_EPIC–CMAQ_BIDI-modeled V_{NH3} to the RFM-reproduced V_{NH3} and find that the ratios are log-normally distributed with a spatial gradient increasing from the north to the south (Figure S8). After log-transformation, the ratios are positively correlated with 2-m temperature (T) ($r = 0.76$, $p < 0.001$), which largely explains the latitudinal gradient—higher ratios in the south due to warmer climates. In addition, the ratios show a positive correlation with near-surface wind speed (W, 10-m wind speed) ($r = 0.05$, $p < 0.001$) and a negative correlation with total precipitation (P) ($r = -0.21$, $p < 0.001$). These correlations warrant inclusion of meteorological variables in the RFM. We use an exponential term as the climate-adjustment factor to account for T, W, and P (Experimental Procedures) following previous studies.[12,43] The enhanced model (i.e., RFM$_C$) explains 95% of the $V_{NH3,AG}$ variance, significantly improved from the previous version. The model predictions resemble the gridded $V_{NH3,AG}$ values simulated by FEST-C_EPIC–CMAQ_BIDI (Figures S9A and S9B). Decomposing the effects of LC and the three climate components (i.e., T, W, and P) shows that T is the dominant factor leading to the $V_{NH3,AG}$ increases. Under RCP4.5, increased T in 2100 leads to a net increase of 34% in $V_{NH3,AG}$, while the changes in W and P lead to decreases in $V_{NH3,AG}$ (−3.3% and −3.4%, respectively). Under RCP8.5, however, RFM$_C$ tends to overestimate the increase in $V_{NH3,AG}$ by 22% in 2100 (Figure S10).

In most studies as well as in RFM$_C$, it is assumed that the long-term T dependency of $V_{NH3,AG}$ over agricultural land follows a similar function as that of natural circumstances, e.g., seabird colonies, where $\ln(V_{NH3})$ is a linear function of $1/T$ as $\Delta\ln(V_{NH3}) = \alpha \cdot \Delta(1/T)$, where the values of α are always negative and differ by LC type (Experimental Procedures).[12,43] The sensitivity of V_{NH3} to T ($S_{V,T}$, denotes the percentage change in V_{NH3} to the absolute change in T) derived from the $V_{NH3} \sim T$ function is inversely proportional to T^2 ($S_{V,T} = -\alpha/T^2$), indicating that V_{NH3} becomes less sensitive to T at higher T levels. Our RFM$_C$ shows an α value of −8,690 K for unirrigated crop, equivalent to an $S_{V,T}$ of 10.2% K^{-1} at 18°C and a slightly lower $S_{V,T}$ (9.8% K^{-1}) at 25°C. The $S_{V,T}$ directly calculated from FEST-C_EPIC–CMAQ_BIDI via a year-by-year comparison shows a very similar $S_{V,T}$ (10.2% K^{-1}) at 18°C but a much lower $S_{V,T}$ (4.7% K^{-1}) at 25°C. The difference between FEST-C_EPIC–CMAQ_BIDI-modeled and RFM$_C$-reproduced $S_{V,T}$ suggests that the $V_{NH3,AG}$ in RFM$_C$ is overly sensitive to T changes at higher T levels (Figure 2). For non-agricultural land, on the other hand, the $S_{V,T}$ obtained from RFM$_C$ and FEST-C_EPIC–CMAQ_BIDI match each other over a wide range of T changes (for RFM$_C$, 9.9%–14.8% and 9.5%–14.1% at 18°C and 25°C, respectively; for FEST-C_EPIC–CMAQ_BIDI, 12.0% and 11.4%, respectively) (Figure S11). The functional difference of ΔT at higher T levels between agricultural and non-agricultural lands reflects LC-determined heterogeneous responses of $V_{NH3,AG}$ to warming and implies that the true response for agricultural land could be oversimplified if directly using the semi-empirical relationship obtained from natural circumstances. Further investigation of the FEST-C_EPIC–CMAQ_BIDI simulations reveals that the climate change under RCP8.5 leads to a

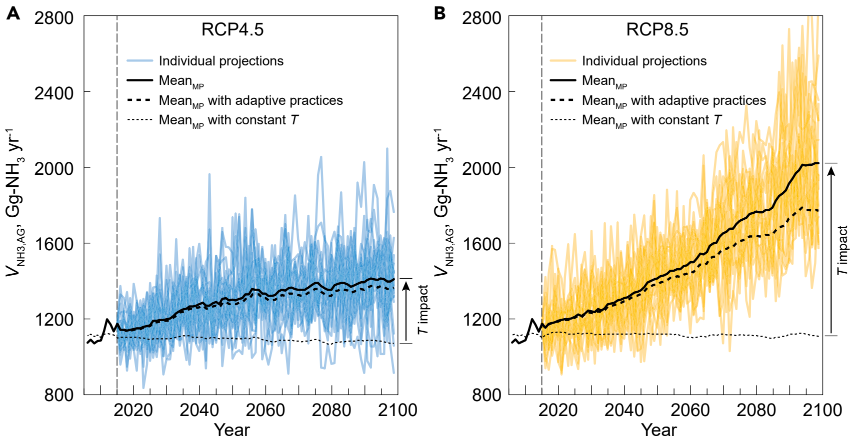

Figure 3. Future Trends of $V_{NH3,AG}$ due to Climate Change

Using the FEST-C_EPIC–CMAQ_BIDI outputs, we develop RFMs via multivariate nonlinear regression analysis. The RFMs are used to (1) decompose the spatial and temporal variations in $V_{NH3,AG}$ associated with land cover types, climate factors, and agricultural management practices, and (2) facilitate multiple projections of $V_{NH3,AG}$. The trends are calculated as multiple projection means based on the RFMs and 18 climate projections under RCP4.5 (A) and RCP8.5 (B). Individual projections, the multiple projection means (Mean$_{MP}$, 5-year running means of multiple projections), the Mean$_{MP}$ with management practices adaptive to climate change, and the Mean$_{MP}$ with T fixed at the 2006–2015 average level are shown in each panel. Harmonization of these projections are conducted to ensure the same historical levels during the period between 2006 and 2015 (Supplemental Experimental Procedures).

decrease of 16.1% in the crop N uptake between 2010 and 2100 due to the extremely warm conditions in 2100. The intense warming under RCP8.5 will inhibit plant growth and development, which is consistent with previous studies.[44,45] In response to the declining crop N demand, FEST-C_EPIC–CMAQ_BIDI reduces the total amount of applied N in 2100 by 15.8% to avoid fertilizer overuse, which suppresses further increases in $V_{NH3,AG}$. On the other hand, the $V_{NH3,AG}$ suppression caused by changing management practices is not captured by RFM$_C$, leading to the overestimation in $V_{NH3,AG}$. To evaluate to what extent management practices can suppress $V_{NH3,AG}$ increases, we conducted a counterfactual simulation where we drove FEST-C_EPIC–CMAQ_BIDI using RCP8.5 2100 climate but fixed the amount of applied N to the 2010 level. The counterfactual simulation shows an overall increase of 85% in $V_{NH3,AG}$, which is 25% higher than the increase in the original simulation where changes in management practices are allowed. The overall difference of $V_{NH3,AG}$ increases between counterfactual and original simulations coincides with the RFM$_C$ overestimation (22%). The analyses consistently show the effect of management practices on $V_{NH3,AG}$ suppression in FEST-C_EPIC–CMAQ_BIDI and imply that the climate dependency of $V_{NH3,AG}$ described by RFM$_C$ is close to a scenario where fixed management practices are adopted irrespective of changing climate.

To reflect the suppression effect of management practices on $V_{NH3,AG}$ under climate warming, we introduce a nonlinear cubic polynomial function in RFM$_C$ to developed RFM$_{C,M}$ (i.e., RFM$_C$ with consideration of the suppression effect of management practices on $V_{NH3,AG}$) (Experimental Procedures). RFM$_{C,M}$ successfully reproduces the $V_{NH3,AG}$ suppression in 2100 under RCP8.5 (Figure S10). Based on RFM$_C$ and RFM$_{C,M}$, we re-projected the future trends of $V_{NH3,AG}$ using high-resolution meteorological fields downscaled from climate projections of 18 climate models,[46,47] isolated the impacts of increases in T, and evaluated the benefits from adopting management practices adaptive to climate change (Figures 3 and 4; Tables S5–S7). All $V_{NH3,AG}$ projections show increasing trends between 2010 and 2100 (Figure 3), with overall increases ranging from +1% (based on GFDL-ESM2G) to +51% (HadGEM2-CC365) under RCP4.5 and from +47% (GFDL-ESM2M) to +128% (HadGEM2-CC365) under RCP8.5 (Tables S6 and S7). Sixteen out of 18 projections show more than 50% increases over at least two-thirds of the CONUS land under RCP8.5, but the changes are not spatially consistent among models (Tables S6 and S7) due to the disparity in projected extents of warming among models. Excluding the impacts of T eliminates the increasing trends (Figure 3) and significantly narrows the variation across projections, indicating the dominant role of warming in future $V_{NH3,AG}$ increases. The multi-projection means show an increase of 285 Gg-NH_3 year^{-1} (95% confidence interval [CI], 222–340 Gg-NH_3 year^{-1}) or 26% (95% CI, 20%–31%) in $V_{NH3,AG}$ between 2010 and 2100 under RCP4.5 and an increase of 900 Gg-NH_3 year^{-1} (95% CI, 767–1,020 Gg-NH_3 year^{-1}) or 81% (95% CI, 69%–92%) under RCP8.5 (see Figure 4 for the spatial distributions of the increases under both climate scenarios). The $V_{NH3,AG}$ increase under RCP8.5 is significantly higher than the single-projection estimate using CESM1. We have found that $V_{NH3,AG}$ accounts for 10% of the total fertilizer N applied in 2010, and the fraction increases to 22% in 2100 under RCP8.5 (if not adopting adaptive management practices). We subsequently evaluate the impacts on crop yield (expressed as N yield in Gg-N year^{-1}), atmospheric burden of NH_3/NH_4^+, and N deposition. Crop yield loss is defined as the reduction in the total yield of the 42 types of crops considered in this study (Table S2) caused by a decrease in the N input and is calculated using the hyperbolic relationship between yield and the effective total N input following previous studies.[48,49] We have found that the $V_{NH3,AG}$ increase is responsible for a 10% loss of total nitrogen applied and a 540 Gg-N year^{-1} loss of crop yields (or 3.7% of the total crop yield), increases the atmospheric burden of NH_3/NH_4^+ by 18% across the CONUS, and enhances the NH_3/NH_4^+ deposition to sensitive ecosystems by 14% (or increases the total N_r deposition to sensitive ecosystems by 8%) (Experimental Procedures) (Figures S12 and S13, see Figure S14 for the definition of sensitive areas). RFM$_{C,M}$ shows that adopting adaptive management practices suppresses the $V_{NH3,AG}$ increase in 2100 only mildly under RCP4.5 (40 Gg-NH_3 year^{-1} or 14% of the $V_{NH3,AG}$ increase) but greatly under RCP8.5 (242 Gg-NH_3 year^{-1} or 27% of the $V_{NH3,AG}$

CellPress
OPEN ACCESS

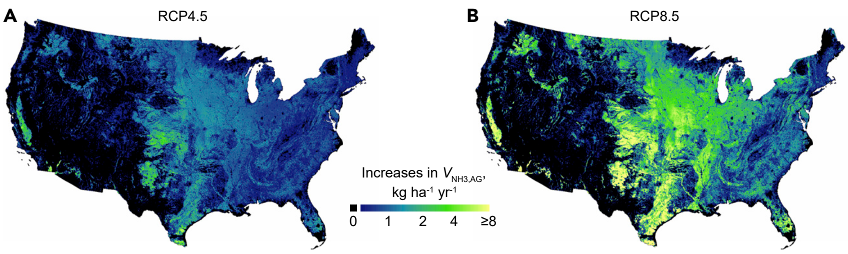

Figure 4. Spatial Distributions of the Increases in $V_{NH3,AG}$ due to Climate Change
Spatial distributions of the $V_{NH3,AG}$ increases due to climate change between 2010 and 2100 under RCP4.5 (A) and RCP8.5 (B). The increases in $V_{NH3,AG}$ are derived based on difference in the ensemble means of 18 $V_{NH3,AG}$ projections between 2010 and 2100 periods.

increase) (Figure 3). Nevertheless, adaptive management practices cannot fully offset the $V_{NH3,AG}$ increase induced by climate change.

Mitigation Strategies

The increasing $V_{NH3,AG}$ under warming urges the need for adopting mitigation strategies that combine adaptive management practices with other feasible mitigation measures. We evaluate the effectiveness of four feasible mitigation measures (Experimental Procedures). Three of the measures (RU, UIR, and UIN) target urea application, which amounts to one-third of $V_{NH3,AG}$. The fourth, DP, is applicable to all types of fertilizers. We have found that full deployment of these individual measures by 2100 (RCP8.5) lowers the $V_{NH3,AG}$ by 500 (RU), 180 (UIR), 280 (UIN), and 700 (DP) Gg-NH_3 year^{-1}, respectively. The most effective strategy, which combines RU and DP with adaptive management practices, reduces the $V_{NH3,AG}$ by 1,186 Gg-NH_3 year^{-1} (59%), where mitigation measures account for 83% of the reduction, and adaptive management practices account for the remaining 17%. The amount of $V_{NH3,AG}$ reduced prevents loss of 13% of applied N, with subsequent crop yield gain of 735 Gg-N year^{-1} (5.0% of the total crop yield), and leads to an 18% decrease in the atmospheric burden of NH_3/NH_4^+ in the CONUS and a 16% decrease in the NH_3/NH_4^+ deposition to sensitive ecosystems (or a 10% decrease in the total N_r deposition to sensitive ecosystems) (Figures S12 and S13).

DISCUSSION

Our study uses a process-based model to project future $V_{NH3,AG}$ trends associated with climate change. We have found that an intense warming (RCP8.5) between 2010 and 2100 will increase the $V_{NH3,AG}$ by ~81% over the CONUS, and that a moderate warming (RCP4.5) can significantly prevent the increasing trend (only an increase of ~26%). All else unchanged, the increases in $V_{NH3,AG}$ will lower agricultural nitrogen use efficiency (NUE). A first-order estimate shows that by the end of 21st century of RCP8.5, the amount of N loss via $V_{NH3,AG}$ over the CONUS will be equal to the amount of crop N yield in California—the largest crop-producing state in the US. While our study focuses on the CONUS, similar $V_{NH3,AG}$ increases are anticipated globally.[19] Mid- and high-latitude regions may see higher $V_{NH3,AG}$ increases due to the greater intensification of regional warming,[50] which warrants further investigation. By the end of the 21st century, the world population will grow by approximately 35%–80%, with food demand increased by 30%–160%.[51–53] The potential decline in NUE due to rising $V_{NH3,AG}$ undermines the efforts to address the need to meet growing food demand, posing a global threat to food security.

Using the process-based model outputs, we develop RFMs to decompose the $V_{NH,AG}$ variations associated with various factors, including LC types, climate factors, and agricultural management practices. The RFM method represents an approach to effectively provide projections of $V_{NH,AG}$ under climate change and modulates the prescribed NH_3 emission inventories that are currently used in most models in a way that takes climate impacts into consideration. However, it is not entirely appropriate to apply our RFMs directly to other world regions. Different parameterizations of the RFMs are expected for different regions given the differences in crop and fertilizer types, climate, soil property, and agricultural practice.[19] Process-based models can be used to translate these regional differences into region-specific parameterizations for RFMs developed by others.

The $V_{NH3,AG}$ increases have far-reaching implications for human and ecosystem health and the global climate because of the significance of the resulting enrichment of atmospheric burden and deposition of NH_3/NH_4^+ species. Our simulations find that not only the boundary layer but also the free troposphere see considerable NH_3/NH_4^+ enrichment owing to the $V_{NH3,AG}$ increases (Figure S15). While in the boundary layer, NH_3 contributes to the formation of secondary aerosols that are associated with adverse health effects,[54] in the free troposphere, the increases in NH_3 may have important implications for cloud formation.[55–57]

Currently, anthropogenic activities inject more than 2-fold N_r to terrestrial ecosystems as natural sources do (190 versus 84 Tg-N year^{-1}).[15] Synthetic fertilizer application dominates the anthropogenic input (~60%), followed by crop N fixation and fossil fuel combustion (~20% each).[15] All else equal, the warming-induced increases in $V_{NH3,AG}$ indicate a greater demand for fertilizer to achieve current crop yield, thereby releasing more N_r to the environment. As it cascades through the environment, the same atom of N transforms into a sequence of different forms and causes multiple effects in series.[58] Adverse impacts of the N cascade are inevitable unless the process is restricted from where the N_r pollution starts.[59] We show that adopting management practices adaptive to climate change and deploying feasible mitigation measures can decrease $V_{NH3,AG}$, and that adaptive management practices will be increasingly more effective as climate warms. The reduction in $V_{NH3,AG}$ caused by implementation of these adaptation actions will fully compensate for the warming-induced increase in $V_{NH3,AG}$ and come along with improved NUEs, maintaining the crop yield while effectively reducing N_r input to terrestrial ecosystems.

We focus on the $V_{NH3,AG}$ increases caused by climate change alone, but $V_{NH3,AG}$ will also grow with global expansion of agriculture and associated fertilizer use driven by growing population and per-capita resource demand.[60,61] In addition to $V_{NH3,AG}$ there are other pathways of N loss that are likely disturbed by climate change, e.g., surface runoff, nitrate leaching, emissions of nitrogen oxide and nitrous oxide from nitrification and denitrification.[62–64] In the context of increasing food demand on top of a changing climate, preventing the unexpected exacerbation of agricultural N loss will require better understanding of the dynamical coupling between human and natural systems, which is the key to integrative process-based modeling of agroecosystems, as demonstrated in part in this study. Extended ground- and space-based measurements are needed to better constrain the magnitudes of N loss from various pathways.[62] The next generation of the process-based models should enable integration of the various pathways of N loss with consideration of multi-media consequences, and incorporation of strategies, technologies, and infrastructure into promising solutions for sustainable development of agriculture.

EXPERIMENTAL PROCEDURES

Resource Availability

Lead Contact

Further information and requests should be directed to and will be fulfilled by the Lead Contact, Huizhong Shen (hshen73@gatech.edu).

Materials Availability

This study did not generate new unique materials.

Data and Code Availability

The source code of FEST-C_EPIC–CMAQ_BIDI can be freely downloaded from the CMAS center at https://www.cmascenter.org/fest-c/ and from ZENODO at https://zenodo.org/record/3585898#.Xu98vWhKg2w. The bias-corrected CMIP5 outputs used to derive the future meteorological fields are available at https://rda.ucar.edu/datasets/ds316.1/. A complete list of fertilizers modeled in FEST-C_EPIC_CMAQ-BIDI are available at https://osf.io/5efua/.

Integrated Model

We use FEST-C v.1.4, CMAQ v.5.3, and an adapted EPIC v.0509, which comprises the most updated version of FEST-C_EPIC–CMAQ_BIDI, to conduct our simulations. EPIC is used to determine the amount and timing of fertilizer application triggered to meet plant demand considering the impacts of both long-term and short-term climate/weather conditions on soil properties and plant growth.[65] CMAQ simulates the transport, full chemistry, and wet and dry deposition of NH_3 and relevant species in the atmosphere.[66] BIDI simulates the air-surface bidirectional fluxes of NH_3.[30] Integrating EPIC and CMAQ, FEST-C enables the dynamic coupling between agriculture and atmosphere at large scales.[30,32]

Downscaled meteorological fields for the periods 2008–2012, 2048–2052, and 2096–2100 under RCP4.5 and RCP8.5 are used to drive the integrated model. The meteorological fields are derived from the bias-corrected outputs of the National Center for Atmospheric Research's CESM1.[39] We use the Weather Research and Forecasting model version 3.8.1[67] with spectral nudging to downscale the global climate projections into the grid containing 120 × 156 horizontal grid cells at the 36-km spatial resolution over the study domain. The downscaling procedure was detailed in a previous study.[68] We use the US EPA's 2011 National Emission Inventory[69] as the baseline emission inventory. To isolate the impact of climate change on $V_{NH3,AG}$, emission sources other than $V_{NH3,AG}$ are kept constant as in the baseline emission inventory across the study periods and climate scenarios. We conduct six 5-year FEST-C_EPIC–CMAQ_BIDI simulations, corresponding to the three periods under the two climate scenarios. We also conduct two real-world simulations and several sensitivity tests to facilitate our analyses. Detailed information about the model setting and the simulation design can be found in Supplemental Experimental Procedures.

Reduced-Form Models

We developed RFMs to predict V_{NH3} using the outputs of the six 5-year FEST-C_EPIC–CMAQ_BIDI simulations as the training database. These RFMs were used to decompose the spatial variations in V_{NH3} into variations in LC and climate factors and to conduct multiple V_{NH3} projections using multi-model climate projections. We used the 4 km-resolution meteorological fields provided by the Multivariate Adaptive Constructed Analogs Datasets to drive the RFMs.[46] Eighteen climate projections under two climate scenarios (RCP4.5 and RCP8.5) were considered in the multi-projection analysis. Detailed information on the model configuration and evaluation, RFM development and parameterization, uncertainty analysis, and the evaluation of the potential impacts of LC change and CO_2 elevation on V_{NH3} can be found in Supplemental Experimental Procedures, Tables S8 and S9.

Mitigation Measures

We chose the four most commonly used mitigation measures and evaluated their individual and combined efficacy in reducing $V_{NH3,AG}$ over the CONUS and resulted beneficial impacts on crop yield, atmospheric burden of NH_3/NH_4^+, and N deposition. The four mitigation measures are RU, UIR, UIN, and DP.[14,48] The $V_{NH3,AG}$ reduction rates of these mitigation measures were directly obtained from a literature review,[14] which, based on a meta-analysis of 824 $V_{NH3,AG}$ measurements, reported reduction rates of 74.5% for RU, 34.5% for UIR, 53.7% for UIN, and 54.7% for DP. We assumed that anhydrous ammonia and nitrogen solution were already deeply placed or injected,[70] and therefore they were not considered when evaluating the mitigation potential of DP. We applied the reduction rates of the first three measures to cropland fertilized with urea only and the fourth to all cropland, and evaluated their efficacy in reducing $V_{NH3,AG}$ separately by region. We chose one of the first three measures accompanying the fourth to evaluate the combined efficacy of two measures. We calculated the $V_{NH3,AG}$ reduction associated with the most effective strategy, which adopts a combination of RU and DP with adaptive management practices.

Impact Assessments

Focusing on RCP8.5, we evaluated the impacts of climate change-induced $V_{NH3,AG}$ increase and mitigation-induced $V_{NH3,AG}$ reduction on crop yield, atmospheric burden of NH_3/NH_4^+ over the CONUS domain, and N deposition to sensitive ecosystems. The crop yield loss due to the $V_{NH3,AG}$ increase and the crop yield gain due to the $V_{NH3,AG}$ mitigation were evaluated based on the hyperbolic relationship between yield and the effective N input following previous studies.[48,49] The changes in the atmospheric burden of NH_3/NH_4^+ and the N deposition were modeled using CMAQ. We used the protected biodiversity areas (GAP Status Code 1 and 2, areas permanently protected for the protection of biodiversity) defined by the Protected Areas Database of the United States as the sensitive areas of interest (Figure S14).[71] Details can be found in Supplemental Experimental Procedures.

SUPPLEMENTAL INFORMATION

Supplemental Information can be found online at https://doi.org/10.1016/j.oneear.2020.06.015.

ACKNOWLEDGMENTS

We thank Ellen Cooter (US EPA, retired) and Verel Benson (Benson Consulting) for their discussions and suggestions. This research is supported by the U.S. Environmental Protection Agency (EPA grant no. R835880) and the National Science Foundation (NSF SRN grant no. 1444745). Its contents are solely the responsibility of the grantee and do not necessarily represent the official views of the supporting agencies. Furthermore, the US government does not endorse the purchase of any commercial products or services mentioned in the publication.

AUTHOR CONTRIBUTIONS

H.S. conceived the idea. H.S. designed the study. A.G.R., Y.H., L.R., and F.Z. provided suggestions on the study design. H.S. and Y.C. conducted the model simulations under the guidance of Y.H., L.R., and J.E.P. H.S. and Y.C. analyzed the results. H.S. wrote the manuscript with input from all authors.

DECLARATION OF INTERESTS

The authors declare no competing interests.

Received: December 7, 2019
Revised: May 31, 2020
Accepted: June 30, 2020
Published: July 24, 2020

REFERENCES

1. Weber, R.J., Guo, H.Y., Russell, A.G., and Nenes, A. (2016). High aerosol acidity despite declining atmospheric sulfate concentrations over the past 15 years. Nat. Geosci. *9*, 282–285.
2. Chen, Y.L., Shen, H.Z., and Russell, A.G. (2019). Current and future responses of aerosol pH and composition in the US to declining SO_2 emissions and increasing NH_3 emissions. Environ. Sci. Technol. *53*, 9646–9655.
3. Seinfeld, J.H., and Pandis, S.N. (2016). Atmospheric Chemistry and Physics: From Air Pollution to Climate Change (John Wiley).
4. Cohen, A.J., Brauer, M., Burnett, R., Anderson, H.R., Frostad, J., Estep, K., Balakrishnan, K., Brunekreef, B., Dandona, L., Dandona, R., et al. (2017). Estimates and 25-year trends of the global burden of disease attributable to ambient air pollution: an analysis of data from the Global Burden of Diseases Study 2015. Lancet *389*, 1907–1918.
5. Boucher, O., Randall, D., Artaxo, P., Bretherton, C., Feingold, G., Forster, P., Kerminen, V.-M., Kondo, Y., Liao, H., Lohmann, U., et al. (2013). Clouds and aerosols. In Climate Change 2013: The Physical Science Basis. Contribution of Working Group I to the Fifth Assessment Report of the Intergovernmental Panel on Climate Change (Cambridge University Press), pp. 571–657.
6. Xu, R., Pan, S., Chen, J., Chen, G., Yang, J., Dangal, S., Shepard, J., and Tian, H. (2018). Half-century ammonia emissions from agricultural systems in Southern Asia: magnitude, spatiotemporal patterns, and implications for human health. GeoHealth *2*, 40–53.
7. Van Breemen, N., Burrough, P.A., Velthorst, E.J., Van Dobben, H.F., De Wit, T., Ridder, T.B., and Reijnders, H.F.R. (1982). Soil acidification from atmospheric ammonium sulphate in forest canopy throughfall. Nature *299*, 548.
8. Bouwman, A., Van Vuuren, D., Derwent, R., and Posch, M. (2002). A global analysis of acidification and eutrophication of terrestrial ecosystems. Water Air Soil Pollut. *141*, 349–382.
9. Behera, S.N., Sharma, M., Aneja, V.P., and Balasubramanian, R. (2013). Ammonia in the atmosphere: a review on emission sources, atmospheric chemistry and deposition on terrestrial bodies. Environ. Sci. Pollut. Res. *20*, 8092–8131.
10. Fangmeier, A., Hadwiger-Fangmeier, A., Van der Eerden, L., and Jäger, H.-J. (1994). Effects of atmospheric ammonia on vegetation—a review. Environ. Pollut. *86*, 43–82.
11. Zhan, X., Bo, Y., Zhou, F., Liu, X., Paerl, H.W., Shen, J., Wang, R., Li, F., Tao, S., Dong, Y., et al. (2017). Evidence for the importance of atmospheric nitrogen deposition to eutrophic Lake Dianchi, China. Environ. Sci. Technol. *51*, 6699–6708.
12. Sutton, M.A., Reis, S., Riddick, S.N., Dragosits, U., Nemitz, E., Theobald, M.R., Tang, Y.S., Braban, C.F., Vieno, M., Dore, A.J., et al. (2013). Towards a climate-dependent paradigm of ammonia emission and deposition. Philos. Trans. R. Soc. B Biol. Sci. *368*, 20130166.
13. Bouwman, A., Boumans, L., and Batjes, N. (2002). Estimation of global NH_3 volatilization loss from synthetic fertilizers and animal manure applied to arable lands and grasslands. Glob. Biogeochem. Cycle *16*, 1024.
14. Pan, B., Lam, S.K., Mosier, A., Luo, Y., and Chen, D. (2016). Ammonia volatilization from synthetic fertilizers and its mitigation strategies: a global synthesis. Agric. Ecosyst. Environ. *232*, 283–289.
15. Battye, W., Aneja, V.P., and Schlesinger, W.H. (2017). Is nitrogen the next carbon? Earth's Future *5*, 894–904.
16. Warner, J., Dickerson, R., Wei, Z., Strow, L., Wang, Y., and Liang, Q. (2017). Increased atmospheric ammonia over the world's major agricultural areas detected from space. Geophys. Res. Lett. *44*, 2875–2884.
17. Skjøth, C., and Geels, C. (2013). The effect of climate and climate change on ammonia emissions in Europe. Atmos. Chem. Phys. *13*, 117–128.
18. Zhou, F., Ciais, P., Hayashi, K., Galloway, J., Kim, D.G., Yang, C.L., Li, S.Y., Liu, B., Shang, Z.Y., and Gao, S.S. (2016). Re-estimating NH_3 emissions from Chinese cropland by a new nonlinear model. Environ. Sci. Technol. *50*, 564–572.
19. Xu, R.T., Tian, H.Q., Pan, S.F., Prior, S.A., Feng, Y.C., Batchelor, W.D., Chen, J., and Yang, J. (2019). Global ammonia emissions from synthetic nitrogen fertilizer applications in agricultural systems: empirical and process-based estimates and uncertainty. Glob. Chang. Biol. *25*, 314–326.
20. Massad, R.-S., Nemitz, E., and Sutton, M. (2010). Review and parameterisation of bi-directional ammonia exchange between vegetation and the atmosphere. Atmos. Chem. Phys. *10*, 10359–10386.
21. Bash, J., Cooter, E., Dennis, R., Walker, J., and Pleim, J. (2013). Evaluation of a regional air-quality model with bidirectional NH_3 exchange coupled to an agroecosystem model. Biogeosciences *10*, 1635–1645.
22. Zhan, X., Chen, C., Wang, Q., Zhou, F., Hayashi, K., Ju, X., Lam, S.K., Wang, Y., Wu, Y., Fu, J., et al. (2019). Improved Jayaweera-Mikkelsen model to quantify ammonia volatilization from rice paddy fields in China. Environ. Sci. Pollut. Res. *26*, 8136–8147.
23. Dari, B., Rogers, C.W., and Walsh, O.S. (2019). Understanding factors controlling ammonia volatilization from fertilizer nitrogen applications, BUL 926 https://www.extension.uidaho.edu/publishing/pdf/BUL/BUL926.pdf.
24. Fowler, D., Steadman, C.E., Stevenson, D., Coyle, M., Rees, R.M., Skiba, U., Sutton, M., Cape, J., Dore, A., Vieno, M., et al. (2015). Effects of global change during the 21st century on the nitrogen cycle. Atmos. Chem. Phys. *15*, 13849–13893.
25. Bai, E., Li, S., Xu, W., Li, W., Dai, W., and Jiang, P. (2013). A meta-analysis of experimental warming effects on terrestrial nitrogen pools and dynamics. New Phytol. *199*, 441–451.
26. Ji, C.J., Yang, Y.H., Han, W.X., He, Y.F., Smith, J., and Smith, P. (2014). Climatic and edaphic controls on soil pH in alpine grasslands on the Tibetan Plateau, China: a quantitative analysis. Pedosphere *24*, 39–44.
27. Jones, M., Leith, I., Fowler, D., Raven, J., Sutton, M., Nemitz, E., Cape, J., Sheppard, L., Smith, R., and Theobald, M. (2007). Concentration-dependent NH_3 deposition processes for mixed moorland semi-natural vegetation. Atmos. Environ. *41*, 2049–2060.
28. Xu, R. (2019). Chapter 8: rise of future ammonia emissions from global croplands. In Anthropogenic and natural disturbances of the nitrogen cycle at multiple scales from local to global: a modeling investigation of nitrous oxide and ammonia emissions (Auburn University), PhD Dissertation https://etd.auburn.edu/handle/10415/6659.
29. Pleim, J.E., Bash, J.O., Walker, J.T., and Cooter, E.J. (2013). Development and evaluation of an ammonia bidirectional flux parameterization for air quality models. J. Geophys. Res. Atmos. *118*, 3794–3806.
30. Pleim, J.E., Ran, L.M., Appel, W., Shephard, M.W., and Cady-Pereira, K. (2019). New bidirectional ammonia flux model in an air quality model coupled with an agricultural model. J. Adv. Model. Earth Syst. *11*, 2934–2957.
31. Ran, L., Cooter, E., Yang, D., Benson, V., Yuan, Y., Hanna, A., and Val, G. (2018). User's Guide for the Fertilizer Emission Scenario Tool for CMAQ (FEST-C) Version 1.4. Community Modeling and Analysis System. https://www.cmascenter.org/fest-c/documentation/1.4/FESTC_v1_4_UserManual.pdf.
32. Ran, L., Yuan, Y., Cooter, E., Benson, V., Yang, D., Pleim, J., Wang, R., and Williams, J. (2019). An integrated agriculture, atmosphere, and hydrology modeling system for ecosystem assessments. J. Adv. Model. Earth Syst. *11*, 4645–4668.
33. Food and Agriculture Organization of the United Nations. (2019). FAOSTAT. http://www.fao.org/faostat/en/#home.

34. Cooter, E.J., Bash, J.O., Benson, V., and Ran, L. (2012). Linking agricultural crop management and air quality models for regional to national-scale nitrogen assessments. Biogeosciences *9*, 4023–4035.
35. Cooter, E., Benson, V., Ran, L., and Yang, D. (2013). EPIC Modeling System for CMAQ 12km Grids in the FEST-C V1.0. EP-W-09-023 (USEPA).
36. European Space Agency. Land cover CCI. http://maps.elie.ucl.ac.be/CCI/viewer/index.php.
37. National Oceanic and Atmospheric Administration (2012). State of the climate: national climate report for annual 2012. https://www.ncdc.noaa.gov/sotc/national/201213.
38. National Atmospheric Deposition Program. Ammonia monitoring network. http://nadp.slh.wisc.edu/amon/.
39. Monaghan, A., Steinhoff, D., Bruyere, C., and Yates, D. (2014). NCAR CESM Global Bias-Corrected CMIP5 Output to Support WRF/MPAS Research (Research Data Archive at the National Center for Atmospheric Research, Computational and Information Systems Laboratory).
40. Robertson, G.P., and Groffman, P. (2007). Nitrogen transformations. In Soil Microbiology, Ecology and Biochemistry, Third Edition (Elsevier), pp. 341–364.
41. Gerik, T.J., Oosterhuis, D.M., and Torbert, H.A. (1998). Managing cotton nitrogen. Adv. Agron. *64*, 115–147.
42. Chauhan, B.S., Jabran, K., and Mahajan, G. (2017). Rice Production Worldwide, *Vol. 247* (Springer).
43. Riddick, S., Blackall, T., Dragosits, U., Tang, Y., Moring, A., Daunt, F., Wanless, S., Hamer, K., and Sutton, M. (2017). High temporal resolution modelling of environmentally-dependent seabird ammonia emissions: description and testing of the GUANO model. Atmos. Environ. *161*, 48–60.
44. Rosenzweig, C., Elliott, J., Deryng, D., Ruane, A.C., Müller, C., Arneth, A., Boote, K.J., Folberth, C., Glotter, M., Khabarov, N., et al. (2014). Assessing agricultural risks of climate change in the 21st century in a global gridded crop model intercomparison. Proc. Natl. Acad. Sci. U S A *111*, 3268–3273.
45. Sánchez, B., Rasmussen, A., and Porter, J.R. (2014). Temperatures and the growth and development of maize and rice: a review. Glob. Chang. Biol. *20*, 408–417.
46. Taylor, K.E., Stouffer, R.J., and Meehl, G.A. (2012). An overview of CMIP5 and the experiment design. Bull. Amer. Meteorol. Soc. *93* (4), 485–498.
47. Abatzoglou, J.T., and Brown, T.J. (2012). A comparison of statistical downscaling methods suited for wildfire applications. Int. J. Climatol. *32*, 772–780.
48. Sanz-Cobena, A., Lassaletta, L., Estellés, F., Del Prado, A., Guardia, G., Abalos, D., Aguilera, E., Pardo, G., Vallejo, A., Sutton, M., et al. (2014). Yield-scaled mitigation of ammonia emission from N fertilization: the Spanish case. Environ. Res. Lett. *9*, 125005.
49. Lassaletta, L., Billen, G., Grizzetti, B., Anglade, J., and Garnier, J. (2014). 50 year trends in nitrogen use efficiency of world cropping systems: the relationship between yield and nitrogen input to cropland. Environ. Res. Lett. *9*, 105011.
50. Pachauri, R.K., Allen, M.R., Barros, V.R., Broome, J., Cramer, W., Christ, R., Church, J.A., Clarke, L., Dahe, Q., Dasgupta, P., et al. (2014). Climate Change 2014: Synthesis Report. Contribution of Working Groups I, II and III to the Fifth Assessment Report of the Intergovernmental Panel on Climate Change (IPCC).
51. Food and Agriculture Organization of the United Nations. Food and agriculture projections to 2050. http://www.fao.org/global-perspectives-studies/food-agriculture-projections-to-2050/en.
52. Bodirsky, B.L., Rolinski, S., Biewald, A., Weindl, I., Popp, A., and Lotze-Campen, H. (2015). Global food demand scenarios for the 21st century. PLoS One *10*, e0139201.
53. United Nations Population Division (2018). World population prospects 2017. https://population.un.org/wpp/Graphs/Probabilistic/POP/TOT/.
54. Kim, K.-H., Kabir, E., and Kabir, S. (2015). A review on the human health impact of airborne particulate matter. Environ. Int. *74*, 136–143.
55. Weber, R., Marti, J., McMurry, P., Eisele, F., Tanner, D., and Jefferson, A. (1996). Measured atmospheric new particle formation rates: implications for nucleation mechanisms. Chem. Eng. Commun. *151*, 53–64.
56. Kirkby, J., Curtius, J., Almeida, J., Dunne, E., Duplissy, J., Ehrhart, S., Franchin, A., Gagné, S., Ickes, L., Kürten, A., et al. (2011). Role of sulphuric acid, ammonia and galactic cosmic rays in atmospheric aerosol nucleation. Nature *476*, 429.
57. Yu, F. (2006). Effect of ammonia on new particle formation: a kinetic H_2SO_4-H_2O-NH_3 nucleation model constrained by laboratory measurements. J. Geophys. Res. Atmos. *111*, D01204.
58. Galloway, J.N., Aber, J.D., Erisman, J.W., Seitzinger, S.P., Howarth, R.W., Cowling, E.B., and Cosby, B.J. (2003). The nitrogen cascade. Bioscience *53*, 341–356.
59. Galloway, J.N., Dentener, F.J., Capone, D.G., Boyer, E.W., Howarth, R.W., Seitzinger, S.P., Asner, G.P., Cleveland, C.C., Green, P., Holland, E.A., et al. (2004). Nitrogen cycles: past, present, and future. Biogeochemistry *70*, 153–226.
60. Tilman, D., Balzer, C., Hill, J., and Befort, B.L. (2011). Global food demand and the sustainable intensification of agriculture. Proc. Natl. Acad. Sci. U S A *108*, 20260–20264.
61. Agrawal, A., Brown, D.G., and Sullivan, J.A. (2019). Are global land grabs ticking socio-environmental bombs or just inefficient investments? One Earth *1*, 159–162.
62. Nevison, C., Andrews, A., Thoning, K., Dlugokencky, E., Sweeney, C., Miller, S., Saikawa, E., Benmergui, J., Fischer, M., Mountain, M., et al. (2018). Nitrous oxide emissions estimated with the CarbonTracker-Lagrange North American Regional inversion framework. Glob. Biogeochem. Cycle *32*, 463–485.
63. Mosier, A., Syers, J.K., and Freney, J.R. (2013). Agriculture and the Nitrogen Cycle: Assessing the Impacts of Fertilizer Use on Food Production and the Environment, *Vol. 65* (Island Press).
64. Tian, H., Yang, J., Xu, R., Lu, C., Canadell, J.G., Davidson, E.A., Jackson, R.B., Arneth, A., Chang, J., and Ciais, P. (2019). Global soil nitrous oxide emissions since the preindustrial era estimated by an ensemble of terrestrial biosphere models: magnitude, attribution, and uncertainty. Glob. Chang. Biol. *25*, 640–659.
65. Williams, J., Jones, C., and Dyke, P.T. (1984). A modeling approach to determining the relationship between erosion and soil productivity. Trans. ASAE *27*, 0129–0144.
66. Byun, D., and Schere, K.L. (2006). Review of the governing equations, computational algorithms, and other components of the models—3 Community Multiscale Air Quality (CMAQ) modeling system. Appl. Mech. Rev. *59*, 51–77.
67. Skamarock, W.C., Klemp, J.B., Dudhia, J., Gill, D.O., Barker, D.M., Duda, M.G., Huang, X.-Y., Wang, W., and Powers, J.G. (2008). A Description of the Advanced Research WRF Version 3. NCAR/TN-475+STR (Mesoscale and Microscale Meteorology Division, National Center For Atmospheric Research).
68. Shen, H., Chen, Y., Li, Y., Russell, A.G., Hu, Y., Henneman, L.R., Odman, M.T., Shih, J.-S., Burtraw, D., Shao, S., et al. (2019). Relaxing energy policies coupled with climate change will significantly undermine efforts to attain us ozone standards. One Earth *1*, 229–239.
69. United States Environmental Protection Agency. (2015). 2011 National Emissions Inventory (NEI) data. https://www.epa.gov/air-emissions-inventories/2011-national-emissions-inventory-nei-data.
70. Wang, Q., Zhou, F., Shang, Z., Ciais, P., Winiwarter, W., Jackson, R.B., Tubiello, F.N., Janssens-Maenhout, G., Tian, H., Cui, X., et al. (2020). Data-driven estimates of global nitrous oxide emissions from croplands. Natl. Sci. Rev. *7*, 441–452.
71. United States Geological Survey. (2018). Gap analysis project (GAP), protected areas Database of the United States (PAD-US): U.S. Geological survey data release. https://doi.org/10.5066/P955KPLE.